AN-92-9-2

5655

EXPERIMENTAL AND NUMERICAL RESULTS FOR AIRFLOW AND PARTICLE TRANSPORT IN A MICROELECTRONICS CLEAN ROOM

T.H. Kuehn, Ph.D., P.E.
Member ASHRAE

D.Y.H. Pui, Ph.D.
Member ASHRAE

J.P. Gratzek

ABSTRACT

This paper presents experimental measurements of time-averaged air velocities, turbulence intensity, and turbulent frequency distribution near an exhaust bench located in a Class 10 side-wall exhaust, tunnel-type clean room. Particle concentration data were also obtained from four particle-source locations using PSL particles of 0.357 and 1.09 micron diameter. A variety of two-dimensional numerical solutions have been obtained for this configuration. Quantitative comparisons are given for time-averaged airflow velocity magnitude and direction and particle concentration. The good agreement between the measured and computed velocity results shows that numerical models can accurately predict the flow pattern in this configuration. However, the particle concentration agreement is not as good.

INTRODUCTION

Numerical models have been used to predict airflows in rooms for nearly 20 years. Only recently have industrial clean room airflows received attention. Much of the equipment and benches in these facilities is designed without detailed consideration of the airflows and associated contaminant transport. The accuracy and reliability of numerical models should be tested to determine which solution methods are most appropriate. This involves comparing results from different solutions to the same problem and comparing these results with experimental data.

An example of a comparison between numerical methods is the study published by De Vahl Davis and Jones (1983) in which 37 contributions from 30 contributors were compared for a simple natural convection cavity flow. A benchmark numerical solution was obtained by the authors, but no experimental comparisons were made.

Numerical solutions for airflow in microelectronics clean rooms have been published by a number of authors including Shanmugavelu et al. (1987). Murakami et al. (1990) included contaminant transport using a convection-diffusion approach. Kuehn (1988) reviewed the appropriate methodology that could be used in clean room airflow and contaminant transport modeling.

Comparisons of numerical solutions and experimental data in clean rooms have been made for a few geometries. Kuehn et al. (1988) presented velocity measurements and flow visualization results in a clean room and compared the data with corresponding numerical solutions with good agreement.

The purpose of this exercise is to clearly define a realistic airflow and particle contamination situation that can be modeled numerically and to compare the numerical solutions to corresponding experimental data. The results should indicate whether numerical solutions can accurately predict the airflow pattern and contamination transport in a real, microelectronics manufacturing clean room.

REVIEW OF THE FLOW-MODELING EXERCISE

The two-dimensional geometry, nature of the flow, boundary conditions, and the location of the particle sources and sampling locations are defined in a clean room flow-modeling exercise. For purposes of simplifying the numerical solution, the flow is assumed to be two-dimensional. A cross section of the aisle with clean bench, particle sources, and sample points is given in Figure 1. Table 1 details the nature of the flow and the boundary conditions for the exercise. The inlet supply air is to be distributed uniformly with a face velocity of 100 fpm (0.51 m/s) in the vertical downward direction with a turbulence intensity of 5%. The ceiling supply air is disrupted by 2 in. (0.05 m) wide streamlined light fixtures placed 2 ft apart. The shield spanning from the ceiling downward to a height 18 in. (0.46 m) above the front edge of the bench is intended to act as a barrier against particles from sources II and IV. The smaller obstruction located inside the shielded area has source III located in the center of its underside. This obstruction acts as a piece of processing equipment that mechanically generates particles. The larger object in the aisle region represents a human obstruction. On the upper left-hand corner of this obstruction is source IV. In addition to these sources, there are two ceiling sources simulating leaks in the

Thomas H. Kuehn is a professor and **David Y.H. Pui** is an associate professor in the Department of Mechanical Engineering, University of Minnesota, Minneapolis. **James P. Gratzek** is a research assistant in the School of Mechanical Engineering, Georgia Institute of Technology, Atlanta.

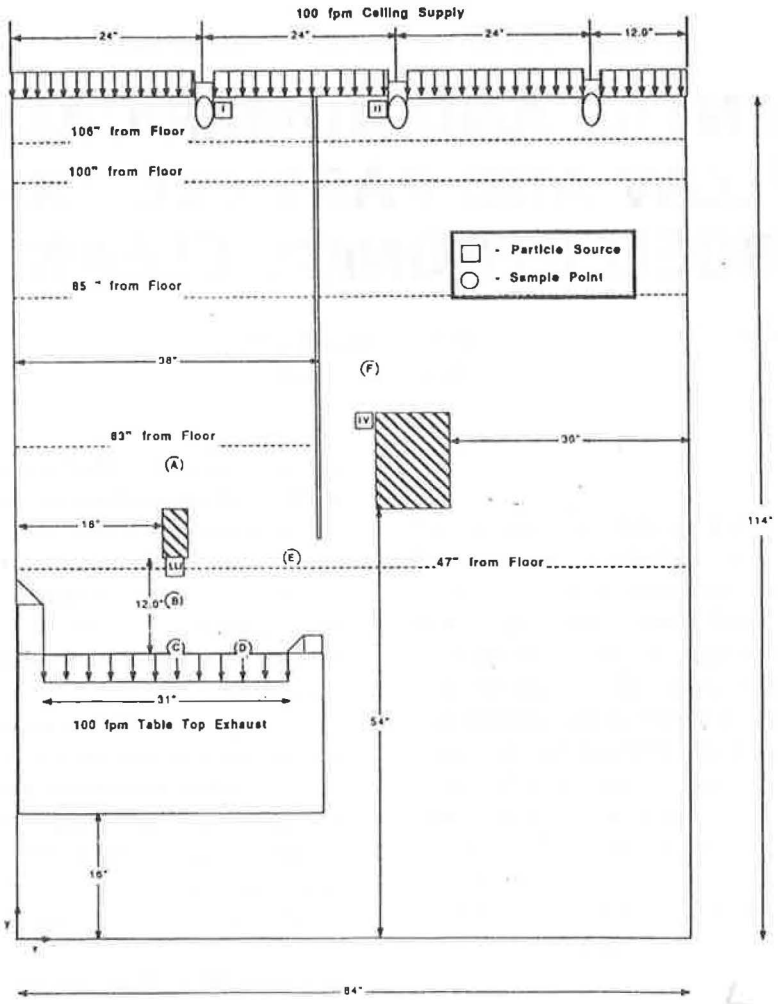

Figure 1 *Geometry and dimensions for the clean room flow-modeling exercise.*

TABLE 1
Nature of Flow and Boundary Conditions

Nature of Flow	Boundary Conditions
• Two-Dimensional	• Ceiling Supply at 100 fpm (0.51 m/s)
• Steady	• Turbulence Intensity at Ceiling Supply is 5%
• Isothermal, T=70°F (21°C)	• Return under Bench along Vertical Wall
• Incompressible	• Centerline of Room is Line of Symmetry
• Negligible Viscous Dissipation	• All Surfaces Stationary Solids
	• Exhaust from Bench Top Uniform at 100 fpm (0.51 m/s)

TABLE 2
Location and Type of Particle Generation Points and Location of Sample Points

Source #	x(in.)	y(in.)	Aerosol	Sample #	x(in.)	y(in.)
I	25	114	HEPA Supply	A	19.5	60
II	47	114	HEPA Supply	B	19.5	42
III	19.5	48	Mechanical Wear	C	27	36
IV	45	66	Human	D	34.75	48
				E	42	72

TABLE 3
Generation Rates for Particle Sources

Particle Size Range (μm)	Mean Particle Size (μm)	Aerosol Generation Rate (num/min/ft) HEPA Supply	Mechanical Wear	Human
0.1-0.5	0.22	16	450	9.9×10^4
0.5-2.0	1.0	22	250	5.0×10^5
2.0-10.0	3.16	1	80	3.8×10^4

HEPA filters—one located inside the shielded region and the other over the aisle. The horizontal surface of the bench acts as an exhaust for a portion of the flow. Its velocity is considered to be downward and uniform at 100 fpm (0.51 m/s). The other outlet is located below the wall under the bench and is 16 in. (0.41 m) in height.

Particle source locations and sample point locations are depicted in Figure 1 as squares and circles, respectively. Their coordinates are given in Table 2. The aerosol type is also listed next to the source coordinates in Table 2. Each particle source has specified generation rates for particles in three size categories. Table 3 gives generation rates for the three size categories for each of the three source types. The coordinate system has its origin at the lower left-hand corner of the room where x is in the horizontal direction and y in the vertical direction. Dimensions are in feet and inches.

EXPERIMENTAL SETUP AND METHODOLOGY

Facility

The measurements were performed in one bay of a class 10 tunnel-type clean room with 100% HEPA filter ceiling coverage except for the teardrop light fixtures. The dimensions and boundary conditions of the bay closely approximate those of the modeling exercise as shown in Figure 1.

The flow is assumed to be two-dimensional. Consequently, the model clean bench, flow obstruction structures, and injection probes were all constructed to simulate a two-dimensional geometry. Figure 2 shows a photograph of the full-scale model clean bench. It was constructed to have a cross section identical to the geometry defined in the exercise. The model bench was 8 ft (2.4 m) long and was constructed of galvanized sheet metal. An 8 ft (2.4 m) high acrylic wall was attached to each end of the bench to ensure two-dimensional flow. Another acrylic shield extended from the ceiling downward to a height 18 in. (0.46 m) above the front edge of the bench, as specified in the exercise. A metal grille was placed over the hollow benchtop. Layers of screen mesh were added to the grille until the benchtop exhaust velocity reached the specified 100 ± 5 fpm (0.51 ± 0.03 m/s).

The "human head" and "robot arm" obstructions were also made of galvanized sheet metal and spanned the entire 8 ft (2.4 m) of the bench.

The clean room ceiling was covered with 2 ft $\times$ 4 ft (0.6 m $\times$ 1.2 m) HEPA filters. The filters were supported by a 4 in. (0.1 m) wide framework on their short (2 ft) sides. A ledge of about 1/2-in. (0.01-m) width extended out from the base of the light fixtures on which the long side of the filters rested. The filters had no protective grille and receded into the ceiling about 1 in. (0.03 m) from the bottom of the framework.

A large framework of telescopic square tubing was also set up around the bench to facilitate both the placement of the particle source and the automatic traverse system. The traverse system consisted of a computer-controlled X-Y scanner that was used to control the movement of both the velocity probe and the particle-sampling tube. The traverse movement was set to an increment between 1/8 and 2 in. (0.003 and 0.05 m).

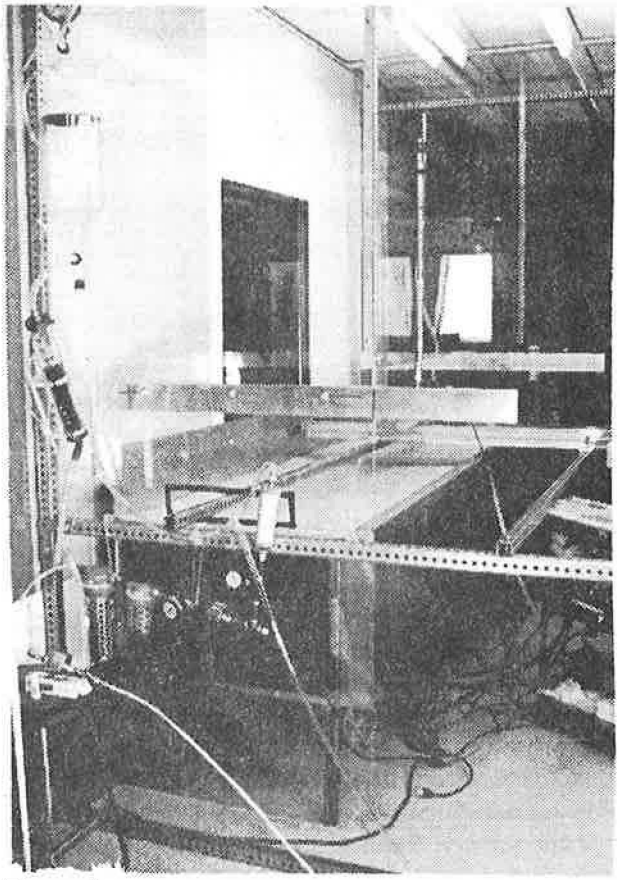

Figure 2 Photograph of bench setup.

Particle Injection Nozzle

A particle injection nozzle was constructed to provide particle sources as specified in the exercise. A two-dimensional model was used in the exercise, and a point source in a two-dimensional problem becomes a line source in a three-dimensional test setup. The design of this "line source" injector is shown schematically in Figure 3. It was made of a copper tube 2 ft (0.6 m) in length and 1/2 in. (0.01 m) in diameter placed within a shell made of thin sheet metal. The shell was bent to a half-circle of 3/4 in. (0.02) I.D. with two parallel 2 in. (0.05 m) straight sections. Both ends of the shell were capped. Particles thus exited through the 3/4 in. $\times$ 2 ft (0.02 m $\times$ 0.6 m) slit opening opposite the closed half-circle. The copper tube axis was centered with the half-circle axis. A row of 1/32 in. (0.8 mm) holes spaced 1/8 in. (3 mm) apart were drilled in the copper tube and were oriented opposite the shell opening. The particle stream thus impacted first with the curved sheet metal and

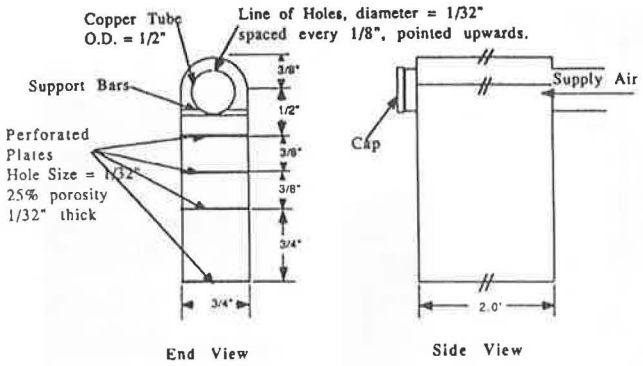

Figure 3 *Particle source nozzle.*

reversed direction to flow around the copper tube toward the shell opening slit. A series of three perforated aluminum plates spaced 3/8 in. (0.01 m) apart, each with 1/32 in. (0.8 mm) holes and 25% porosity, were placed in the shell channel below the tube. The bottom edge of the nozzle was also covered with another perforated aluminum plate. The purpose of these plates was to distribute the particles uniformly across the length of the nozzle and to damp out the turbulence generated within the nozzle.

Figure 4 shows the lengthwise variation of the nozzle velocity for two upstream pressure settings. The velocity profile was nearly uniform over the 1-ft (0.3-m) length of the center section. Further, the widthwise profile was measured to be very uniform across the entire nozzle. Figure 5 shows the lengthwise variation of aerosol concentration exiting the nozzle. The variation of aerosol concentration was measured to be less than 7% from end to end. These results indicate that the nozzle was satisfactory for the experiment, particularly when the measurements were made near the center section of the slit nozzle.

Air Velocity and Turbulence Measurements

Airflow measurements were accomplished in two ways. An omnidirectional hot wire anemometer was used to determine average velocities. The anemometer allowed for averaging over 20-second intervals, which was necessary for the highly fluctuating flow. A single-wire hot wire anemometer with signal conditioning capability was used to measure the instantaneous velocity. The turbulence intensity was computed from

$$TI = \sqrt{\overline{(U')^2}}/\overline{U}.$$

The output was read by a high-speed AD converter interfaced with a personal computer. The system was capable of sampling up to 12 kHz. The velocity probe placement was facilitated by a computer-controlled and automatic scanning system that could be moved within a 2 ft × 4 ft (0.6 m × 1.2 m) area.

Particle Generation and Measurements

Monodisperse polystyrene latex (PSL) particles of several different sizes were generated and transported to the injection nozzle. Figure 6 shows a schematic diagram of the aerosol generation and delivery system. A high-flow-rate nebulizer was used to spray an aqueous suspension of PSL particles. The aerosol was sent through a diffusion dryer and a charge neutralizer and was subsequently diluted in a large mixing chamber with dry nitrogen. The nitrogen stream was also used to adjust the nozzle flow velocity, which was monitored by a pressure gauge. The nozzle flow velocity was set to the same velocity as the clean air velocity from the HEPA filters. As will be seen later, the HEPA velocity fluctuated significantly over the entire length of the nozzle. The nozzle velocity was subsequently adjusted to the "average" velocity from the HEPA filter to approximate the isokinetic condition.

Particle concentration was measured using a laser particle counter, with a lower detection limit of 0.3 μm and a sampling flow rate of 0.1 ft^3/min (2.8 L/min). A

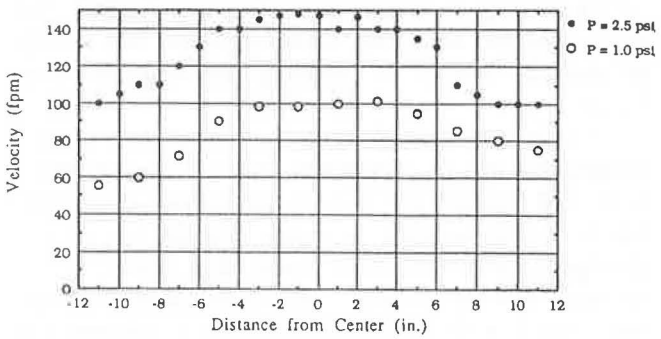

Figure 4 *Variation of nozzle velocity across length of nozzle for upstream pressures of 2.5 and 1 psig.*

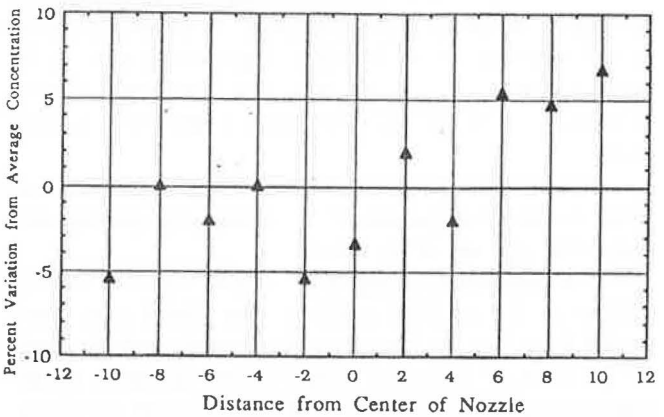

Figure 5 *Variation from average particle concentration across nozzle (average taken as mean of all measurements); pressure = 1 psig, particle diameter = 0.357 μm.*

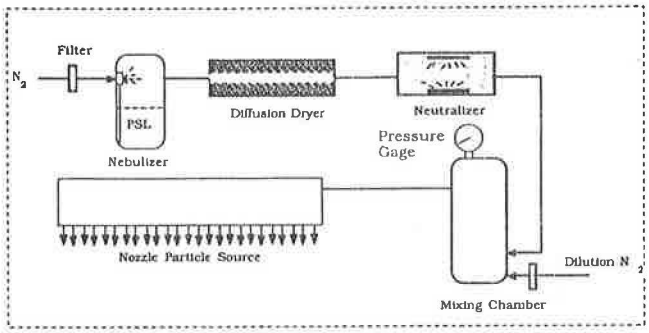

Figure 6 *Aerosol generation and delivery system.*

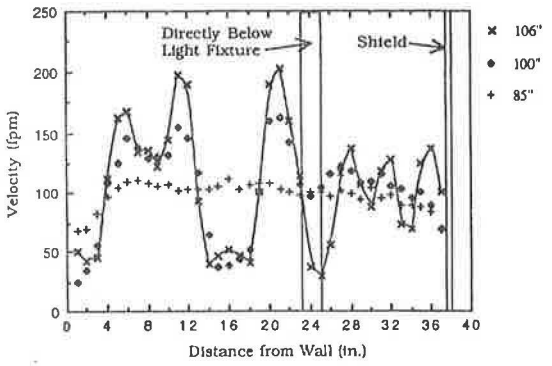

Figure 7 *Velocity profile development above the center of the clean bench at 85, 100, and 106 in. (2.2, 2.5, and 2.7 m) above the floor.*

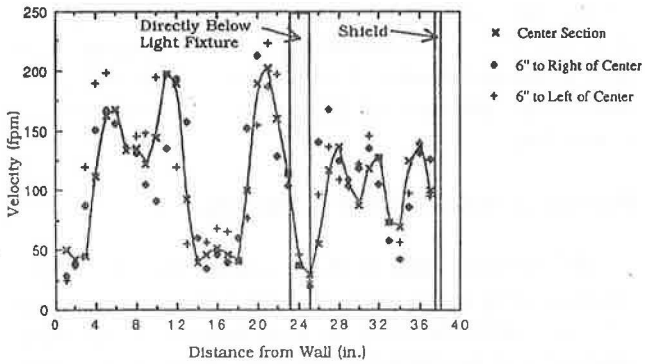

Figure 8 *Velocity profile below HEPA filter 106 in. (2.7 m) from floor (8 in. [0.2 m] below ceiling) for region above the exhaust bench.*

sampling inlet was chosen to give an inlet suction velocity of 100 fpm (0.51 m/s), which gave the isokinetic sampling condition for most test areas. Each run began with a measurement of particle concentration immediately below the nozzle and subsequently scanned the particle concentration at appropriate heights. After the completion of the scan, the source concentration was again measured. Each measurement was taken over 60 seconds in 10-second intervals, or 0.1 ft^3 (2.8 L) total sampling volume.

EXPERIMENTAL RESULTS AND DISCUSSION

Velocity Profiles

Figure 7 shows the velocity profiles as a function of distance from the wall at three elevations from the floor. The data were taken at the centerline of the clean bench width. Considerable fluctuations of the velocity profiles are seen for the two positions immediately below the HEPA filters, i.e., 106 in. and 100 in. (2.69 m and 2.54 m) from the floor (8 in. and 14 in. [0.2 m and 0.36 m] below the filter). The velocity profile continues to develop and becomes nearly uniform at 85 in. (2.2 m) from the floor (29 in. [0.74 m] below the filter). The average velocity at this elevation is approximately 95 fpm (0.48 m/s), which is quite close to the 100 fpm (0.51 m/s) velocity stated in the exercise. Since all the sample points are below this elevation, they experience an average velocity of the approaching flow close to the specified value.

Figure 8 examines the velocity profile immediately below the HEPA filter (8 in. [0.2 m] below the filter) in more detail. In addition to the centerline values, two additional profiles were taken that are located 6 in. (0.15 m) to the right and to the left of the centerline. It is seen that all three profiles give substantially the same velocities at all distances from the wall. The centerline data, therefore, provide a good approximation to the two-dimensional model. The profile shows a rather large oscillation, ranging from less than 50 fpm (0.24 m/s) to more than 200 fpm (1.0 m/s) at some locations. Some of the oscillations can be explained. For example, the presence of the light fixture causes a suppression at approximately 25 in. (0.63 m) from the wall. Other suppressions, such as that at 16 in. (0.4 m) from the wall, have no apparent upstream obstructions. As will be seen later, the analysis of the turbulence level shows that it is likely to be caused by the three-dimensional flow experienced by the single-wire hot wire anemometer. The three-dimensional flow may originate at the pleated HEPA filter. The pleating may cause a nonuniform pressure drop to develop across the filter with resulting vortices formed immediately below the filter.

Turbulence Intensity

Figure 9 shows the RMS velocity as a function of distance from the wall at three elevations above the floor. The RMS velocity divided by the average velocity gives the turbulence intensity in percent. As expected, the RMS velocity measured immediately below the filter gives the largest values, while further away, the RMS velocity reduces to 15 to 20 fpm (0.08 to 0.10 m/s). Since the average velocity is approximately 100 fpm (0.5 m/s), the turbulence intensity of 20% to 60% is extremely high and may indicate the measurement of three-dimensional flow, i.e., recirculating flow, by the single-wire hot wire anemometer.

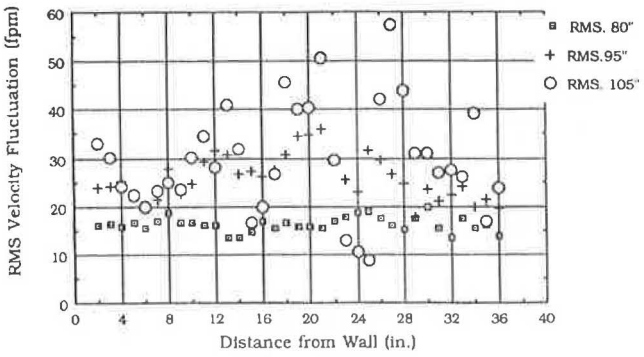

Figure 9 *RMS velocity fluctuation taken at 80, 95, and 100 in. (2.0, 2.4, and 2.5 m) above the floor for the region above the exhaust bench.*

Figure 10 shows the FFT analysis of the turbulent energy spectrum at 29 in. (0.74 m) below the filter measured by the anenometer. The dominant frequency is seen to occur between 1 and 3 Hz, which again may indicate the presence of large mixing vortices and unsteady flow.

Particle Concentration and Dispersion

Polystyrene latex (PSL) particles of three sizes, corresponding to the mean particle sizes of the specified size intervals in the exercise, were generated. Their concentrations at the sample points were measured by a two-channel laser particle counter (LPC). Due to the very low particle concentration for the largest size category (3 to 10 μm) and the high concentration of interfering residue particles from the nebulizer, we were not successful in obtaining data for the largest size category. Consequently, only results for particles of 0.357 μm and 1.09 μm diameter were obtained. The measured particle concentrations are tabulated and discussed in the next section.

Particle dispersions from various sources were also measured. Figure 11 shows particle dispersion at several locations downstream of the particle source. The particle source was injected at position 1 of the exercise adjacent to the light fixture. The distance from the source was equal to 114 in. (2.9 m) minus the stated distance from the floor. The indicated concentration has been normalized with respect to the source concentration. As expected, the particle concentration profile closest to the source (100 in. [2.54 m] from the floor) shows a very high peak with narrow spread. The peak decreases and the profile broadens with distance from the source. Similar results were observed from other particle source locations.

Flow and Particle Data at Sampling Points

Table 4 summarizes the measured velocity and turbulence results at the sample points specified in the exercise. The magnitude, direction, turbulence intensity,

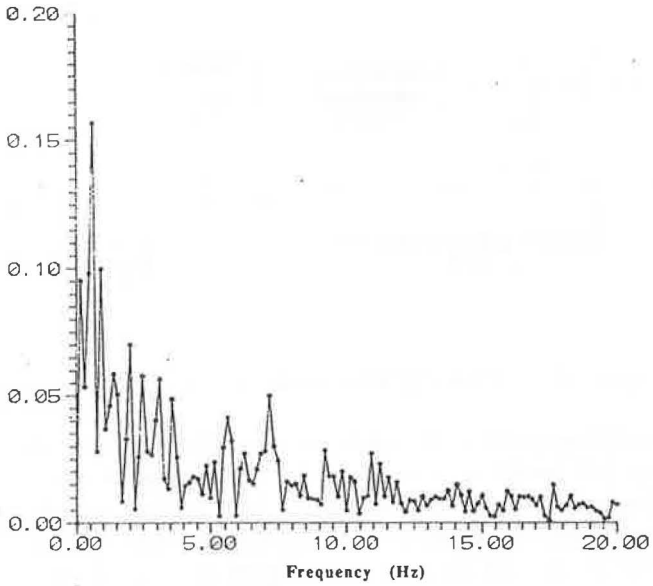

Figure 10 *Fast Fourier transform of velocity signal at 29 in. (0.74 m) below center of filter.*

and dominant frequency for each point are listed. The average velocity represents the average of three readings taken at the centerline plus two locations spaced 6 in. (0.15 m) from the centerline. Each reading represents the average value of more than 30 seconds. The directional information for the flow was obtained using noncontaminating fog, which indicated unsteady oscillating flow under the benchtop obstruction. The directional information could not be obtained for Point B because a recirculation region was observed below the "robot."

Table 5 summarizes the measurement results of particle concentration at various sample points specified in the exercise. Note that the concentrations have been normalized with particle generation rates specified in the exercise, and no effort was made to correct for the three-dimensional effects. The actual generation rates were much higher in the experiment than those specified in the

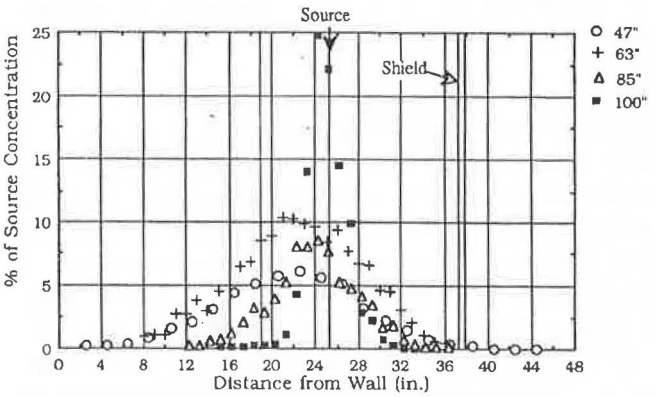

Figure 11 *Dispersion from HEPA source #1 at 47, 63, 85, and 100 in. (1.2, 1.6, 2.2, and 2.5 m) from floor; particle diameter = 0.357 μm.*

TABLE 4
Experimental Velocity Information at Sample Points

	Sample Point					
	A	B	C	D	E	F
Magnitude (fpm)	85	50	105	95	104	50
Direction* (degrees)	+5 to -5 Unsteady.	In recirculation region. Unsteady.	-5	0	-10	+5
R.M.S. Velocity Fluctuation	14%	28%	11%	7%	8%	40%
Dominant Frequency (Hz)	1-3 Hz	1-3 Hz	1-3 Hz	1-3 Hz	1-3 Hz	1-3 Hz

* positive measured clockwise from downward vertical

exercise, as this allowed for much shorter sampling times than would otherwise be necessary. Table 5 represents particle concentration from each source individually at each sample point and then gives a total for each point for all the sources operating simultaneously. The total represents the concentration at each source if all the sources were active at once. Note that the bulk of the total concentration is from source III, the "robot."

NUMERICAL RESULTS

Table 6 presents the essential features of the six numerical solutions. The solutions have been classified with submittal numbers, assigned in no special order, and will be referred to by this submittal number throughout this paper. Of the six solutions submitted, five used finite difference methods while one used a finite element approach to solve for the flow field. With the exception of two solutions that modeled the flow using a uniform viscosity or zero equation turbulence model, turbulence in all of the remaining models was computed using the two-equation k-ε method. All submittals solved the primitive variable equations; none solved for stream function and vorticity. Grid spacing was different in each solution. The total number of control volumes ranged from 1,254 to 6,817. Particle transport was modeled using either the Eulerian or the Lagrangian approach. Most of the solutions solved for simultaneous dispersion from all the sources specified in the exercise.

TABLE 5
Experimentally Determined Particle Concentration
(particles/ft^3)

	Sample Point											
	A		B		C		D		E		F	
Particle Source	Particle Size Range (μm)											
	.1-.5	.5-2	.1-.5	.5-2	.1-.5	.5-2	.1-.5	.5-2	.1-.5	.5-2	.1-.5	.5-2
#1 HEPA I	0.14	.20	0.13	0.17	0.11	0.16	0.13	0.17	0.04	0.05	0.0	0.0
#2 HEPA II	0.0	0.0	0.0	0.0	0.0	0.0	0.0	0.0	0.002	0.002	0.31	0.43
#3 Robot	0.0	0.0	17.4	9.7	7.0	3.9	1.1	0.6	0.0	0.0	0.0	0.0
#4 Human	0.0	0.0	0.0	0.0	0.0	0.0	0.0	0.0	0.0	0.0	0.0	0.0
Total	.14	.20	17.53	9.87	7.11	4.06	1.23	0.77	.042	.052	.31	.43

TABLE 6
Comparison of Solution Methods for the Six Submittals

Submittal Number	Solution Class	# Control Volumes X x Y	Solution Technique for Flow	Turbulence Model	Particle Transport Model	Type of Flow and Source Considered
#1	Finite Difference	47 x 44	Line by Line	Uniform viscosity 100 x μ	Eulerian	Turbulent w/ Sources I, II, III, IV
#2	Finite Difference	39 x 48	Simplified Marker and Cell Method	κ-ε	Eulerian	Turbulent w/ Sources I, II, III, IV
#3	Finite Element	6817 Elements 7130 Nodes	Simultaneous Iteration for Velocity and Pressure Correction	κ-ε	Lagranglan Monte Carlo	Turbulent w/ Source III
#4	Finite Difference	56 x 56	Line by Line	κ-ε	Lagrangian	Turbulent w/ Sources I,II, III, IV
#5	Finite Difference	50 x 47	Line by Line	κ-ε	Eulerian	Turbulent w/ Sources I, II, III, IV
#6	Finite Difference	33 x 38	Line by Line	None	Eulerian	Laminar w/ Sources I, II, III, IV

Figure 12 gives representative plots for the distribution of time-averaged air velocity and distribution of turbulent kinetic energy. Figure 13 shows contours of particle concentration for each of the four individual sources.

COMPARISON WITH EXPERIMENTAL DATA

Table 7 lists the average and range of the numerical solutions and the experimentally measured mean flow velocity and direction at the six sample points. The agreement is generally very good except for sample points B and F. The vortex under the robot obstruction over the bench causes unstable flow in the vicinity of sample point B. It is unclear whether any of the numerical solutions have accurately simulated this flow separation region. The other discrepancy is the measured and computed velocity magnitude at sample point F. The air velocity entering the experimental clean room was highly nonuniform under the HEPA filters. Therefore, the assumed uniform inlet velocity of 100 fpm (0.51 m/s) was not achieved in the experiments. This is the main reason that the experimental velocity magnitude at point F is considerably lower than all the predicted values.

The measured and computed particle concentrations are listed at the six sample points in Table 8. At sample points B, G, and E, the measured values lie within the range of the computed values. At sample points A, D, and F, the data are larger than any of the predictions. The flow is well mixed at sample points B and C, which are in the wake region beneath the robot. Thus, the concentration gradients should be small and coarse flow and particle transport modeling should provide good results. Sample points A and F are near the HEPA filter. The nonuniformities in the measured flow near the ceiling are likely to cause considerably more mixing than would be predicted from the problem statement. Therefore, it is not surprising that the measurements at these two locations show larger particle concentrations than the solutions. The measured particle concentrations at sample point D are also larger than the computed values. This may be caused by a difference in particle dispersion below the HEPA filters near source I or different flow conditions near sample point D.

DISCUSSION

The good agreement in airflow results indicates that numerical modeling of fluid flow is quite accurate for a configuration such as the clean room considered here. Comparisons of the sample point results for experimental and numerical velocity data show good agreement in magnitude with an average deviation of 21%. Directional information does not agree quite as well. This could be

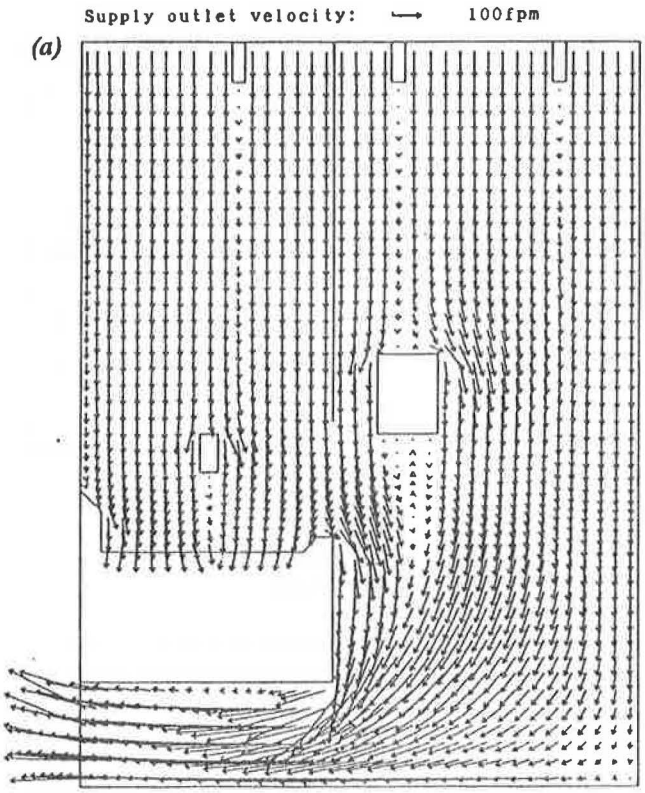

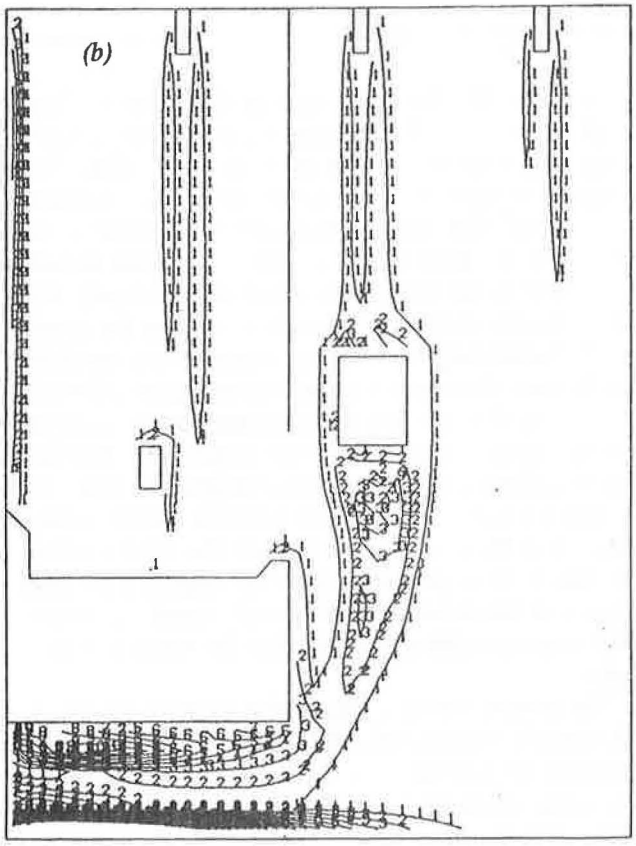

Figure 12 *Mean air velocities (a) and turbulent kinetic energy contours (b).*

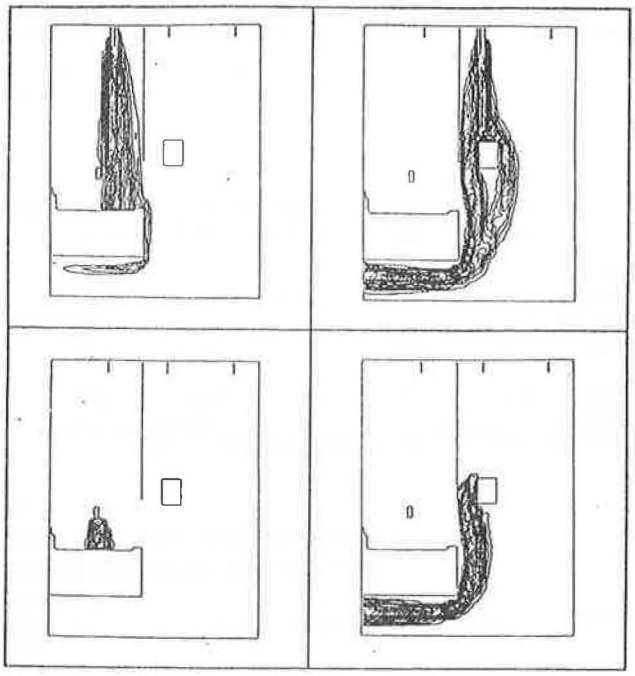

Figure 13 *Particle concentration contours from each source (submittal #4).*

the result of a number of causes. For the sample points located below the robot, numerical solutions disagree. Inappropriate mesh-size selection may be the cause of this. Experimental measurements are also subject to greater error when taken in recirculating zones or other wake regions because relatively greater velocity changes occur over smaller distances than in the free stream. Proper probe placement is therefore critical in wake regions. Experimental measurement of the velocity at point F outside the work area was significantly different from numerical values, the difference primarily caused by the nonideal airflow entrance conditions above this region. Flow direction was determined experimentally using fog. Flow disturbances caused either by the presence of the fog source or inherent in the flow made it difficult to determine precisely the flow direction at many of the points. Two-channel hot wire anemometry measurements might help to discern the cause of the unsteadiness. Turbulence measurements and the associated frequency analysis indicate slow frequency, large intensity velocity fluctuation nearly everywhere in the clean room, particularly near the ceiling. Shear layers at the ceiling may be responsible for unsteady flow conditions. Whether velocity measurements indicate just unsteadiness (laminar unsteady flow) or unsteadiness and mixing (turbulent flow) and to what extent are still uncertain. This phenomenon needs to be investigated further.

Comparison of particle concentrations at each of the sample points shows some agreement in relative magnitude at all of the sample points. Of particular interest is the greater spread measured experimentally. For HEPA source I, particles were detected experimentally at all of

TABLE 7
Comparison of Numerically and Experimentally Generated Velocity Information at the Sample Points Shown in Figure 1

	Sample Point											
	A		B		C		D		E		F	
	Air Velocity Magnitude (fpm)	Dir.* (deg)	Magnitude (fpm)	Dir. (deg)	Magnitude (fpm)	Dir. (deg)	Magnitude (fpm)	Dir. (deg)	Magnitude (fpm)	Dir. (deg)	Magnitude (fpm)	Dir. (deg)
Numerical Average	87.7	-4.2	37.7	-5.75	85.5	-4.2	99.9	11	103.8	-7.3	87.6	5.6
Numerical Range	4.9	6.36	26.6	17.9	35.8	33.9	14.6	9.2	17.7	6.55	8.4	5.1
Exper. Values	85	+5to-5	50	un-steady	105	-5	95	0	104	-10	80	5

* direction measured clockwise from downward vertical

TABLE 8
Comparison of Numerically and Experimentally Generated Concentration at the Sample Points for All Sources Generating Simultaneously for Three Particle Size Ranges
(Concentration in num/ft^3)

	Sample Point																	
	A			B			C			D			E			F		
	Particle Size Range (μm)																	
	.1-.5	.5-2	2-10	.1-.5	.5-2	2-10	.1-.5	.5-2	2-10	.1-.5	.5-2	2-10	.1-.5	.5-2	2-10	.1-.5	.5-2	2-10
Numerical Average	.01	.01	.001	21.8	12.1	11.1	8.2	4.6	0.1	0.16	0.001		1.2	6.0	0.4	0.06	0.06	0.003
Range	0.4	.06	.005	26.6	14.5	39.3	10.6	5.9	0.2	0.24	0.03		6	30	2	0.2	0.2	0.01
Exper. Values	.14	.20	---	18	10	---	7	4	---	1.2	.8	---	.09	.05	---	.3	.4	---

*-Source III only

the shielded sample points, A, B, C, D, and E. None of the numerical solutions except one predicted the presence of particles at point A. This suggests that the actual plume tended to move more toward the wall (to the left) than the solutions predicted. This may be due to the fact that the ceiling supply and benchtop exhaust are not in the proper proportion but is likely due to the fact that the entrance conditions are nonuniform. There does not appear to be a significant difference between the Eulerian and Lagrangian particle-modeling approaches. One would expect the two methods to agree when correct particle turbulent diffusivity is used in the Eulerian model and the particles do not experience significant inertia, gravitational force, or electrostatic force. These conditions are met in this clean room application but may not be met in other aerosol applications. However, the disagreement between the various numerical solutions and the lack of agreement with the experimental data suggest that further aerosol model refinements are necessary to accurately predict particle concentrations in applications similar to this clean room.

CONCLUSIONS

Experimental measurements indicate some inflow boundary conditions that differ from those proposed in the exercise. On the other hand, agreement between much of the experimental and numerical results makes a fairly strong argument for continued simulation effort. The agreement between velocity results from the numerical solutions and the experimental data was found to be within 20% for most of the locations considered regardless of the numerical solution approach utilized. The particle results exhibited more variation, but the trends agreed qualitatively between the solutions and the data. Particle concentration prediction requires accurate knowledge of the flow conditions in addition to an accurate particle transport model. Perhaps large-scale, low-frequency eddies cause more particle dispersion than predicted using a conventional two-equation k-ε turbulence model. The flow conditions beneath the HEPA filters were much more nonuniform in the experiments than assumed in the exercise, which could result in considerably larger particle dispersion than the solutions would predict.

The present exercise shows that existing numerical codes can adequately predict the airflow in an at-rest clean room with no buoyancy. A more realistic model would consider the entire three-dimensional flow field. Transient effects, such as wafer carrier movement, robot motion, and operator movement, will generate additional large-scale air motion, which will result in significantly larger particle transport. Buoyant flows from hot objects or

chemical vapors will also affect the flow. These additional simulation features should be included to predict the particle contamination expected in operating manufacturing environments more closely.

CONTRIBUTORS OF NUMERICAL SOLUTIONS

Fardi, B., Intel, Rio Rancho, NM.

Forbes, S., Assistant Professor, Mechanical Engineering Department, University of Akron, Akron, OH.

Han, H., Assistant Professor, Mechanical Engineering Department, Kookmin University, Seoul, Korea.

Reinders, R., Interatom GmbH, Bergisch Gladbach, West Germany.

Suzuki, M., Ryowa Air-Conditioning and Refrigeration Co. Ltd., Tokyo, Japan.

Tsuzuki, K., J. Kobayashi, T. Iino, and M. Ikegawa, Mechanical Engineering Research Laboratory, Hitachi Ltd., Ibaraki, Japan.

ACKNOWLEDGMENTS

Financial support of this research has been provided by the Particulate Contamination Control Research Consortium at the University of Minnesota. The assistance of the Microelectronics and Information Sciences Center at the University of Minnesota is gratefully acknowledged.

REFERENCES

De Vahl Davis, G., and I.P. Jones. 1983. Natural convection in a square cavity: A comparison exercise. *International Journal for Numerical Methods in Fluids* 3: 227-248.

Kuehn, T.H. 1988. Computer simulation of airflow and particle transport in clean rooms. *Journal of Environmental Sciences* (September/October) XXXI: 21-27.

Kuehn, T.H., V.A. Marple, H. Han, D. Liu, I. Shanumgavelu, and S. Youssef. 1988. Comparison of measured and predicted airflow patterns in a clean room. *Proceedings, Institute of Environmental Sciences*: 331-336.

Murakami, S., S. Kato, and Y. Suyama. 1990. Numerical study of flow and contaminant diffusion fields as affected by flow obstacles in conventional-flow-type clean room. *ASHRAE Transactions* 96(2).

Shanmugavelu, I., T.H. Kuehn, and Y.H. Liu. 1987. Numerical simulation of flow fields in clean rooms. *Proceedings, Institute of Environmental Sciences*: 298-303.